$KCrF_3$: Electronic structure and magnetic and orbital ordering from first principles

Gianluca Giovannetti,[1,2] Serena Margadonna,[3] and Jeroen van den Brink[1,4]
[1]*Institute Lorentz for Theoretical Physics, Leiden University, P.O. Box 9506, 2300 RA Leiden, The Netherlands*
[2]*Faculty of Science and Technology and MESA+ Institute for Nanotechnology, University of Twente, P.O. Box 217, 7500 AE Enschede, The Netherlands*
[3]*School of Chemistry, University of Edinburgh, West Mains Road, Edinburgh EH9 3JJ, United Kingdom*
[4]*Institute for Molecules and Materials, Radboud Universiteit Nijmegen, P.O. Box 9010, 6500 GL Nijmegen, The Netherlands*
(Received 24 July 2007; revised manuscript received 17 October 2007; published 13 February 2008)

The electronic, magnetic and orbital structures of $KCrF_3$ are determined in all its recently identified crystallographic phases (cubic, tetragonal, and monoclinic) with a set of *ab initio* local spin density approximation (LSDA) and LSDA+U calculations. The high-temperature undistorted cubic phase appears as a metal from LSDA, but it is a Mott insulator with a gap of 1.72 eV at the LSDA+U level. The tetragonal and monoclinic phases of $KCrF_3$ exhibit cooperative Jahn-Teller distortions concomitant with staggered $3x^2-r^2/3y^2-r^2$ orbital order. We find that the energy gains due to the Jahn-Teller distortion are 82 and 104 meV per chromium ion in the tetragonal and monoclinic phases, respectively. These phases show A-type magnetic ordering and have a band gap of 2.48 eV. In this Mott insulating state, $KCrF_3$ has a substantial conduction bandwidth leading to the possibility for the kinetic energy of charge carriers in electron- or hole-doped derivatives of $KCrF_3$ to overcome the polaron localization at low temperatures, in analogy with the situation encountered in the colossal magnetoresistive manganites.

DOI: 10.1103/PhysRevB.77.075113 PACS number(s): 71.45.Gm, 71.10.Ca, 71.10.−w, 73.21.−b

I. INTRODUCTION

About a decade ago, the discovery of the colossal magnetoresistance (CMR) effect in doped manganites caused a surge of interest in these perovskite oxides.[1,2] The particular physical properties of the CMR materials are related to the fact that their parent compound $LaMnO_3$ contains Mn^{3+} ions with four electrons in its d shell. On the one hand, the presence of these Jahn-Teller active ions leads to a strong coupling between the electrons and the lattice, giving rise to polaron formation which is widely perceived to be essential for the CMR effect.[3,4] On the other hand, when doped, the d^4 high spin state leads, via the double exchange mechanism, to a ferromagnetic metallic state with a large magnetic moment, making the system easily susceptible to externally applied magnetic fields.[5]

The presence of strong electron correlations and an orbital degree of freedom, to which the Jahn-Teller effect is directly related, adds to the complexity and gives rise to an extraordinarily rich phase diagram at higher doping concentration, displaying a wealth of spin, charge, orbital, and magnetically ordered phases.[6,7] Thus, the high spin d^4 state of Mn^{3+} is intimately related to a plethora of physical phases, effects, and properties. However, it is important to note that the high spin d^4 state is *not* exclusive to trivalent manganese.

Formally, high spin Cr^{2+} is electronically equivalent to Mn^{3+}. However, due to its low ionization potential divalent chromium is rarely found in solid state systems. $KCrF_3$ is a rare and intriguing example. Recently, we characterized in detail the temperature-dependent crystallographic phase diagram of $KCrF_3$, revealing strong structural, electronic, and magnetic similarities with $LaMnO_3$,[8,9] including the presence of Jahn-Teller distortions, orbital ordering and orbital melting at high temperature. Here, we report *ab initio* electronic structure calculations on the different phases of this compound, within both the local spin density approximation (LSDA) and the LSDA+U, in which local electron correlation effects are partially accounted for. The results of our calculations clearly show that $KCrF_3$ and $LaMnO_3$ are not only structurally but also electronically very similar.

$KCrF_3$ displays three different crystallographic structures, see Fig. 1. At very high temperatures, the system is a cubic perovskite (space group Pm-$3m$).[9] Below 973 K, the JT-active high spin Cr^{2+} ion induces a lattice distortion to a body-centered tetragonal unit cell (space group $I4/mcm$), isostructural to the Cu^{2+} analog, $KCuF_3$. In the tetragonal phase, the CrF_6 octahedra are distorted, leading to short Cr-F bonds along the c axis and alternating long-short Cr-F bonds in the ab plane, indicative of the presence of a staggered type of orbital ordering. On cooling below 250 K, there is a phase transition to a more complicated monoclinic structure with space group $I2/m$.

From our density functional calculations, we find that the tetragonal phase of $KCrF_3$ is a strongly correlated insulator with a gap of 0.49 eV in LSDA and 2.48 eV in LSDA+U (with $U=6$ eV). For this value of U, the calculated relaxed lattice structure is in excellent agreement with the experimental one. In the tetragonal orbitally ordered phase, we find a crystal-field splitting between the Cr t_{2g} and e_g states of 1.0 eV and a total energy gain related to the Jahn-Teller splitting of the e_g states of 0.328 eV per unit cell containing four chromium ions. The cooperative Jahn-Teller distortion is accompanied by A-type antiferromagnetic spin ordering in a similar fashion to $LaMnO_3$.[10–13] We find a magnetic moment of 3.85 μ_B per Cr^{2+} ion, in excellent agreement with experiment, and in-plane and out-of-plane superexchange parameters of -2.6 and 3.4 meV, respectively.

The system displays antiferrodistortive ordering of the $3d_{3x^2-r^2}$ and $3d_{3y^2-r^2}$ orbitals in the ab plane—an ordering motif very different from the orbital ordering in $KCuF_3$

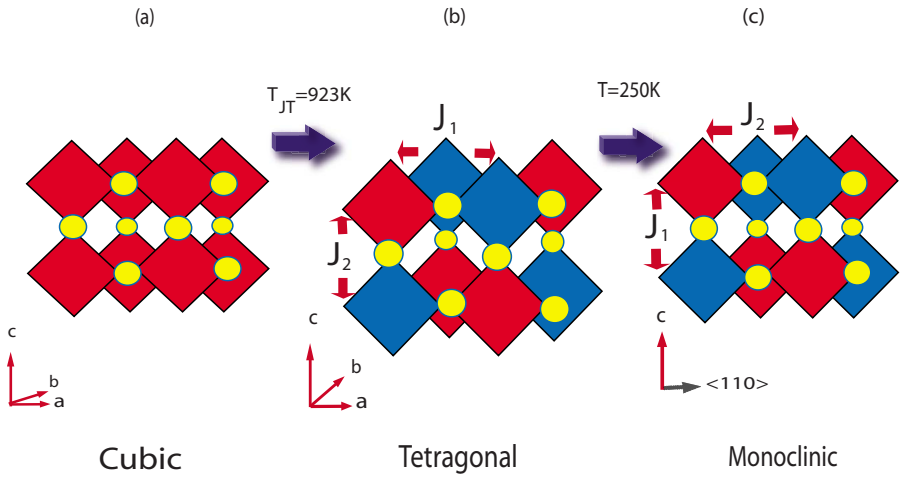

FIG. 1. (Color online) (a) Cubic perovskite crystal structure of $KCrF_3$ at high temperature. (b) Schematic representation of the intermediate-temperature tetragonal structure with CrF_6 octahedra elongated in an alternate fashion. (c) Schematic representation of the low-temperature monoclinic structure. In both the tetragonal and monoclinic structures, we find an A-type magnetic ground state. The ferromagnetic planes are antiferromagnetically stacked along the c axis in the tetragonal case and along the $\langle 110 \rangle$ axis in the monoclinic structure.

that gives rise to a quasi-one-dimensional spin chain formation and rather resembles the orbital ordering in $LaMnO_3$.[10–17] Along the c axis, the orbital ordering pattern in $KCrF_3$ is rotated by 90° in consecutive layers. This in contrast to the manganite where the ordering along the c axis is a uniform repetition of the in-plane orbital structure. Another difference with $LaMnO_3$ is that the e_g bandwidth in the chromium compound, as computed within LSDA, is smaller. However, this is partially compensated in LSDA+U, which shows a bandwidth of the lower Hubbard e_g band of 1.0 eV.

On cooling below 250 K, $KCrF_3$ shows a phase transition to a more complicated monoclinic structure (space group $I2/m$) with four chromium atoms in the unit cell. Our calculations show that in the monoclinic phase, an A-type magnetic structure is also realized and that the Jahn-Teller energy is lowered, leading to an even stronger orbital ordering. However, the resulting electronic gap and magnetic moment of the compound barely change.

In the following, we will present the electronic structure calculations for the three different crystallographic structures. For each one, we considered several possible magnetic ordering structures (ferromagnetic and antiferromagnetic of A, G, and C types) and analyzed the resulting electronic properties, Jahn-Teller energies, and orbital orderings.

II. INTERMEDIATE-TEMPERATURE TETRAGONAL PHASE

The structural changes which occur on lowering the temperature below 973 K through the cubic-to-tetragonal phase transition can be described in terms of two components: a uniform Q_3-type tetragonal distortion, which shortens one lattice constant (along the c direction with Cr-F bonds of 2.005 Å) and lengthens the other two (along the a and b directions), and a Q_2-type staggered distortion, which introduces alternating Cr-F bond lengths in the ab plane with two distinct Cr-F bonds of 2.294 and 1.986 Å. This is a textbook example of a cooperative Jahn-Teller distortion of e_g type on a three-dimensional cubic lattice.[18] The lattice parameters of the resulting body-centered tetragonal unit cell at room temperature are $a=6.052\,30$ Å and $c=8.021\,98$ Å.[8]

The self-consistent calculations that we will present next are done within LSDA (Ref. 19) and LSDA+U using the Vienna *ab initio* simulation package (VASP),[21] within the density functional theory using the exchange-correlation potential of the Ceperly-Alder[20] form. Total energies for the tetragonal structure were calculated with a kinetic cutoff energy of 500 eV and the tetrahedron with Blochl correction using 105 irreducible k points.

A. Local spin density approximation electronic structure of tetragonal $KCrF_3$

We start our study of the tetragonal structure of $KCrF_3$ at the LSDA level and then proceed to also include local correlations within LSDA+U. We find that the A-type antiferromagnetic spin ordered structure is the ground state. The band structure and the (projected) density of states (DOS) are shown in Fig. 2. The system is insulating with an energy gap of 0.49 eV, which is induced by the Jahn-Teller splitting of the e_g states. In accordance with Hund's rule, the Cr^{2+} ions are in a high spin $t_{2g}^3 e_g^1$ state, giving rise to a magnetic moment of $3.59\mu_B$ per Cr.

The Fermi level lies just above the bands with t_{2g} and e_g characters, in agreement with the high spin state of the Cr ions. The exchange splitting is about 2.6 eV, which moves the minority-spin bands far above the Fermi level. The t_{2g}-e_g crystal field splitting Δ_{CF} is about 1.0 eV. The occupied Cr bands show little dispersion along the Γ-Z direction and are therefore of quasi-two-dimensional character, which is due to the specific ordering of the e_g orbitals that maximizes hybridization in plane and minimizes the out-of-plane dispersion. The character of occupied e_g bands is mixed between the two

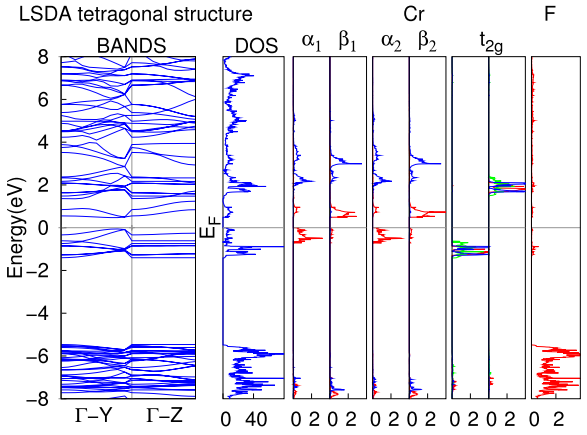

FIG. 2. (Color online) Band structure and projected density of states calculated in LSDA for the tetragonal structure of $KCrF_3$. Majority and minority (red and blue), respectively contributions to the DOS (per unit cell) for Cr ions and the average over all the F ions for p orbitals in the range of [0:4] are plotted. Projected density of states corresponding to t_{2g} orbitals d_{xy}, d_{yz}, d_{xz} of Cr ions are shown in the inset (red, green, blue) with majority and minority contributions toward the left and right, respectively. The labels α_i, β_i label the states $3x^2-r^2$, y^2-z^2 and $3y^2-r^2$, x^2-z^2 for the different Cr 1 and 2 sites in the ab plane.

types of e_g states but mainly comes from $3x^2-r^2, 3y^2-r^2$ orbitals on neighboring Cr ions. This becomes immediately clear from the contour plot of charge density corresponding to the e_g bands below the Fermi level, shown in Fig. 3. The orbital ordering is found to be staggered along the c direction and the unoccupied orbitals have $3d_{y^2-z^2}$ and $3d_{x^2-z^2}$ characters, respectively. The chromium compound follows the general rule that in insulating Jahn-Teller systems, elongated orbitals are occupied, and not the planar e_g ones. This rule is understood to be due to the anharmonic lattice effects.[22]

The t_{2g} projected density of states resolved for orbital character shows that the xy states have a different distribution in energy from the twofold degenerate orbitals of yz, zx characters, in agreement with crystal-field symmetry expectations. The bandwidth of the t_{2g} bands is 0.85 eV, while the

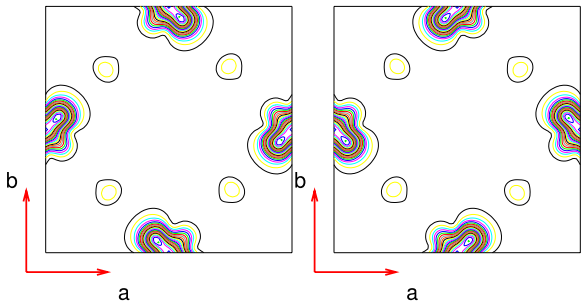

FIG. 3. (Color online) Contour plot of charge density corresponding to the occupied e_g bands within the LSDA for the tetragonal structure of $KCrF_3$. The orbital ordering pattern is clearly seen along the bonds connecting the Cr ions, with $3d_{3x^2-r^2}$ and $3d_{3y^2-r^2}$ alternating in the ab plane. The left and right panels are two cuts on consecutive planes along the c direction.

Jahn-Teller split $e_g{}^1$ bands just below and above the Fermi level each have a width of about 0.65 eV, smaller than the value of 1.0 eV in $LaMnO_3$.[12] However, the inclusion of local correlations within LSDA+U changes this bandwidth significantly.

B. LSDA+U electronic structure of tetragonal $KCrF_3$

It is well known that the incorporation of local Coulomb interactions is essential to understand the physical properties of transition metal compounds.[2] In LSDA+U, the electron-electron interaction is dealt with on a mean field level and we repeated the LSDA calculations above within this scheme.

We performed calculations for a series of values of the on-site Coulomb parameter U, namely, U=2.0, 4.0, 6.0, 8.0 eV, adopting a value for Hund's exchange of J_H =0.88 eV. In practice, the exact definition of U in a solid is not trivial. The value that is found for this parameter depends on, for instance, the precise choice of the orbitals that are used in the calculation.[23–25] In order to determine its value, we performed a structural optimization as a function of U and subsequently stay with the value for U for which we find an equilibrium structure that matches the experimental one. This scheme to extract the Coulomb parameter is viable because the on-site Hubbard U determines for a large part the orbital polarization of the e_g states, which, in turn, causes the structural Jahn-Teller lattice distortion.[16]

Hund's exchange parameter J_H, in contrast, represents a local multipole and is only very weakly screened in the solid and therefore close to its bare atomic value. For it, we used the value for a high spin d^4 configuration determined by constrained density functional calculations.[12] At any rate, small changes of J_H will not affect the results of LSDA+U significantly, as U is the dominating parameter.

To determine U to be used in our calculations, we optimized the three inequivalent Cr-F distances in the tetragonal unit cell, d_1, d_2, and d_3, while fixing the lattice parameters a, b, and c by minimizing the total energy until the changes of total energy are less than 10^{-5} eV and the remaining forces are less than 1 meV/Å. The results are shown in Fig. 4. For U=6.0 eV, we find that the computed structure is very close to the one obtained experimentally, motivating us to adopt this value as the most reliable one. The obtained U value agrees well with that for Mn^{4+} in $LaMnO_3$ [8.0 eV (Ref. 12)] calculated within a constrained LDA+U scheme. In $KCuF_3$, a value of 7.5 eV is similarly found for Cu^{2+}.[16] As one expects that the ionic core potential of Cr^{2+} causes the d electrons to be less localized with respect to both examples above, it is reasonable to find the smaller value of U =6.0 eV for $KCrF_3$.

Below 46 K, antiferromagnetic spin ordering is observed.[8] To study the magnetic exchange couplings between the Cr ions, we calculated the total energy of various magnetic structures. The different magnetic structures we considered are A type (the spins are parallel in the ab planes and the spins are antiparallel along the c axis), F type (all spins parallel), C type (each spin is antiparallel to all others in the ab plane but parallel along the c axis), and G type (every spin is antiparallel to all its neighbors).

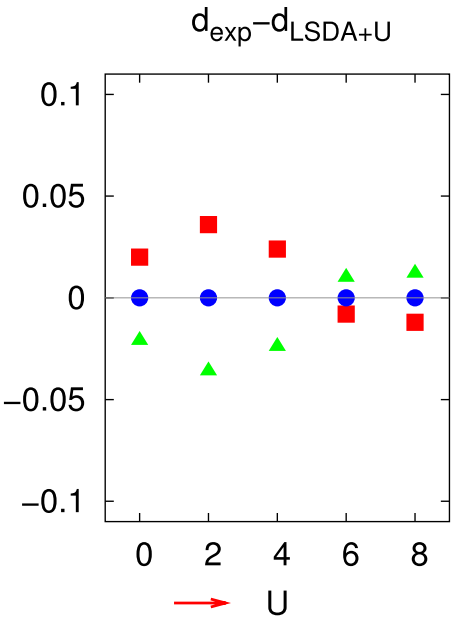

FIG. 4. (Color online) Deviation of relaxed Cr-F distances d_1, d_2, and d_3 from the experiment as a function of the Coulomb interaction U.

From the computations, we find that the ground state is A-type spin ordered for all values of U. The difference in energies between the various magnetically ordered structures for LSDA and LSDA+U is reported in Table I. We analyzed the exchange interactions in the tetragonal unit cell using the Heisenberg Hamiltonian: $\Sigma_{\langle ij\rangle} J_{ij} \mathbf{S}_i \cdot \mathbf{S}_j$. We have calculated the parameters J_{ij} associated with $3d$ states of Cr atoms using the energy of the different magnetic configurations computed in our calculations.

The Heisenberg exchange interactions between spin magnetic moments can be calculated from total energy calculations. J_1 and J_2 being the in-plane and the interplane coupling in the tetragonal unit cell respectively. Note that our sign convention is opposite of the one of Ref. 11. We find (taking into account that in the unit cell there are four Cr ions) $J_1=-2.6$ meV, while $J_2=3.4$ meV (see Fig. 1) for LSDA+U ($U=6.0$ and $J_H=0.88$). These quantities can be compared with the exchange constants of $LaMnO_3$,[11] where $J_1=-9.1$ meV and $J_2=3.1$ meV.

In Fig. 5, the resulting band structure and density of states for the tetragonal structure of $KCrF_3$ within LSDA+U ($U=6.0$ and $J=0.88$ eV) are shown. The LSDA band gap of 0.49 eV increases to a value of 2.48 eV ($U=6.0$ eV), see Table I.

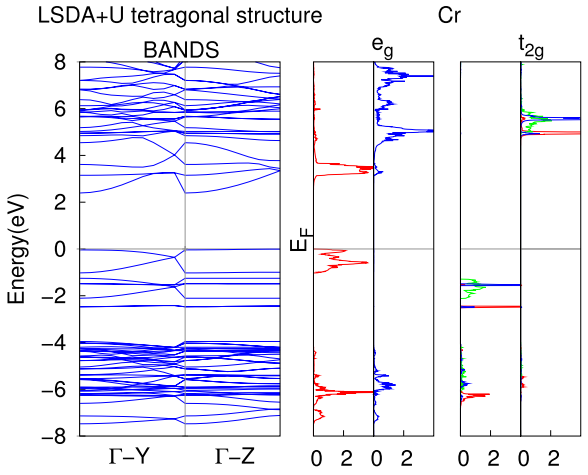

FIG. 5. (Color online) Band structure calculated in LSDA+U with $U=6.0$ and $J=0.88$ eV for the tetragonal structure of $KCrF_3$ and (projected) densities of states. Majority and minority contributions to the DOS (per unit cell) from e_g (red and blue) respectively and t_{2g} (d_{xy}, d_{yz}, d_{xz} in red, green, blue) states for Cr ions in the range of [0:4] toward the left and right, respectively, are plotted.

From the projected density of states, we see that within LSDA+U around the Fermi level, there is a clean distribution of the e_g states $3x^2-r^2/3y^2-r^2$, depending on the Cr site, see Fig. 6. A concomitant enhancement of the orbital polarization is visible in the contour plot of the charge density of the occupied e_g bands, see Fig. 7. This plot also shows that there is an increase in hybridization between the Cr e_g states and fluoride p states which enhances the total bandwidth of the occupied Cr $3de_g$ bands to about 1.0 eV, while the bandwidth of occupied Cr $3dt_{2g}$ bands is about 1.2 eV. The two-dimensional character of the occupied e_g bands does not change in the LSDA+U treatment, but the dispersion of the empty e_g states comes to the fore more clearly. From the computations on the cubic phase in the next section, it will be particularly clear that the two-dimensional character of the occupied e_g bands that is caused by the orbital ordering is also the driving force behind the A-type magnetic ordering, as can be expected on the basis of the Goodenough-Kanamori[10] rules for superexchange.

III. HIGH-TEMPERATURE CUBIC PHASE

In the cubic Pm-$3m$ structure ($a=4.231\,783$ Å),[9] the distances between all Cr and neighboring F ions are equal to

TABLE I. Energy difference (eV) between the magnetic ground state (A type) and other magnetic orderings, band gap Δ (eV), and magnetic moment (μ_B) of the Cr ions in $KCrF_3$.

U	J_H	F type	C type	G type	Δ	μ
0.0	0.00	0.0103	0.4449	0.4791	0.49	3.58
2.0	0.88	0.0343	0.2690	0.2476	0.81	3.63
4.0	0.88	0.0289	0.1303	0.1051	1.73	3.72
6.0	0.88	0.0206	0.0747	0.0553	2.48	3.85
8.0	0.88	0.0141	0.0474	0.0339	3.33	3.98

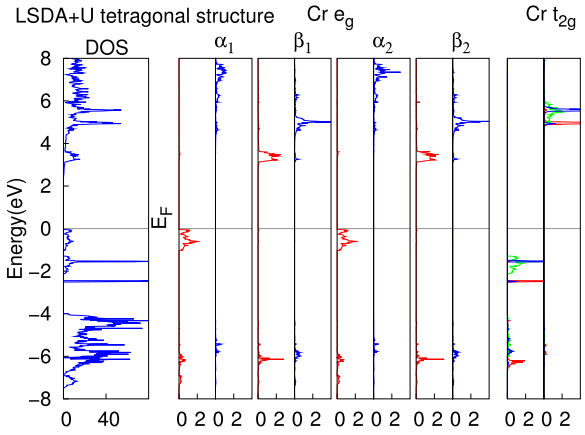

FIG. 6. (Color online) DOS (per unit cell) projected on different Cr d orbitals, calculated in LSDA+U with U=6.0 and J=0.88 eV for the tetragonal structure of $KCrF_3$. Majority and minority contributions to the DOS for Cr ions and the average over all the F ions for p orbitals in the range of [0:4] toward the left and right, respectively, are plotted. The labels α_i, β_i label the states $3x^2-r^2$, y^2-z^2 and $3y^2-r^2$, x^2-z^2 for the different Cr 1 and 2 sites in the ab plane. Projected density of states corresponding to t_{2g} orbitals d_{xy}, d_{yz}, d_{xz} of Cr ions are shown in the inset (red, green, blue).

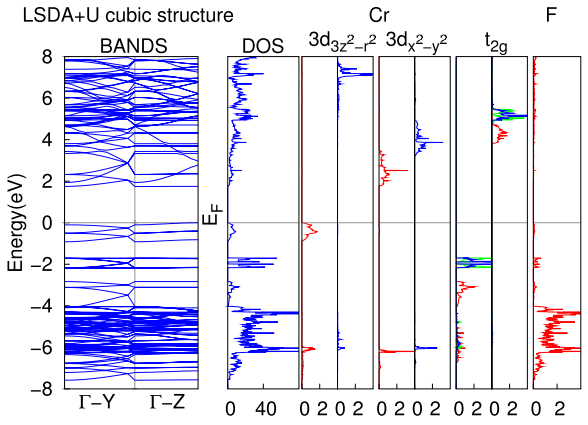

FIG. 8. (Color online) LSDA+U (U=6.0 and J_H=0.88 eV) band structure and projected DOS (per unit cell) for cubic $KCrF_3$ with Pm-3m symmetry and A-type magnetic ordering. Majority and minority contributions to the DOS for Cr ions and the average over all the F ions for p orbitals in the range of [0:4] toward the left and right, respectively, are plotted. Projected density of states corresponding to t_{2g} orbitals d_{xy}, d_{yz}, d_{xz} are shown in the inset (red, green, blue).

2.116 Å and the e_g states are locally degenerate. We find that at the LSDA level, cubic $KCrF_3$ is metallic for the ground state A-type magnetic structure. Such is expected because in the absence of a Jahn-Teller distortion, the e_g band is half-filled even though it is fully spin polarized.

In LSDA+U, a band gap of 1.72 eV opens up—the band structures calculated by LSDA+U (U=6.0 and J=0.88 eV) with the cubic unit cell with A-type magnetic ordering is shown in Fig. 8. The correlation-induced Mott gap is smaller than the charge gap in the tetragonal structure because of the absence of the Jahn-Teller distortion.

Despite the fact that the Jahn-Teller distortions are absent in this structure, there is still an orbital ordering which is due to the magnetic exchange, see Fig. 9. This exchange-driven orbital ordering can be understood in terms of the orbital dependence of the superexchange energy between neighboring Cr sites. Such a situation is described in terms of a Kugel-Khomskii model.[26] For the A-type magnetic ordering, we obtain a homogeneous orbital occupation of $3z^2-r^2$ states, oriented perpendicular to the ferromagnetic plane. This is in accordance with the Goodenough-Kanamori[10] rules for superexchange: bonds of occupied $3z^2-r^2$ orbitals on top of each other have a large overlap, and therefore result in antiferromagnetic spin ordering. Within the plane, the overlap is mainly between occupied $3z^2-r^2$ and empty x^2-y^2 orbitals, causing a ferromagnetic orientation of the spins.

When we consider C-type magnetic ordering, the resulting orbital ordering (see Fig. 9) is of the homogeneous x^2-y^2 type—again with antiferromagnetic spin orientation for

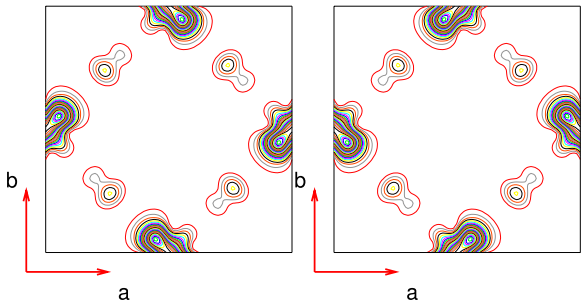

FIG. 7. (Color online) Contour plot of charge density corresponding to the occupied e_g bands within LSDA+U for U=6.0 and J=0.88 eV for the tetragonal structure of $KCrF_3$.

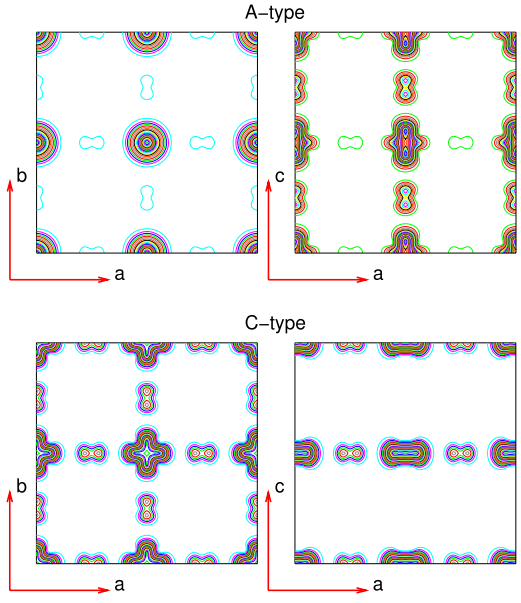

FIG. 9. (Color online) Orbitals in the cubic phase of $KCrF_3$, obtained with LSDA+U. Orbital ordering of $3z^2-r^2$ orbitals for A-type spin ordering and orbital ordering of x^2-y^2 orbitals for C-type spin ordering.

orbitals with lobes pointing toward each other (x^2-y^2 orbitals in the plane) and ferromagnetic orientation between orbitals with small overlap.

The A- and C-type orders that we considered are just two of the many possible magnetic orderings with concomitant orbital orderings: other configurations can appear when the unit cell is doubled or quadrupled in accordance with model calculations on the Kugel-Khomskii Hamiltonian.[26–29] These observations of magnetically driven orbital ordering (or orbitally driven magnetic ordering, depending on one's point of view), although interesting from a theoretical perspective, are not directly relevant to the experimental situation because at the high temperatures where the cubic phase is stable, no long range magnetic ordering is expected. By comparing the total energies of the cubic and tetragonal phases in the nonmagnetic state, we can directly compute the energy gain in the tetragonal phase that is due to the Jahn-Teller distortion alone. We obtain a value of $\Delta E_{JT}=0.328$ eV per unit formula, which is comparable to that found in $LaMnO_3$ (0.504 eV).[13]

IV. LOW-TEMPERATURE MONOCLINIC PHASE

Below 250 K, $KCrF_3$ shows a phase transition to a monoclinic structure, characterized by a pronounced tilting of the CrF_6 octahedra. The lattice parameters at 150 K are $a=5.826\,42$ Å, $b=5.835\,17$ Å, $c=8.575\,47$ Å, and $\gamma=93.686°$.[8] This structure is drastically different from the tetragonal one: it has inequivalent Cr^{2+} sites and shows alternating short and long (2.296 and 1.997 Å, and 2.311 and 1.983 Å, respectively) Cr-F bonds occurring in the plane defined by the c axis and the $\langle 11-0\rangle$ base diagonal. The motif is rotated by 90° in consecutive layers along the $\langle 11-0\rangle$ direction (in which Cr-F bond lengths are 2.018 and 2.001 Å). We construct a magnetic supercell with 80 ions and we performed the total energy calculations with a kinetic cutoff energy of 500 eV and used the tetrahedron method with Blochl correction using 90 irreducible k points. The resulting bandstructure is shown in Fig. 10.

The total energy that we compute in the monoclinic phase reveals that the Jahn-Teller distortion is further stabilized with an energy gain of 22 meV per Cr with respect to the tetragonal phase. Again, in the LSDA+U calculations, the magnetic ground state is found to be A type (in this magnetic structure, Cr^{2+} sites are coupled antiferromagnetically along the $\langle 11-0\rangle$ direction), the Cr moment is $3.85\mu_B$, the band gap is 2.49 eV, and the orbital ordering is essentially the same as in the tetragonal phase (see Fig. 11). Per unit formula, the ferromagnetic configuration is higher in energy by 0.0168 eV, the C-type configuration by 0.0438 eV, and the G-type state by 0.0275 eV.

From this, we find the in-plane and interplane magnetic couplings $J_1=-2.1$ meV and $J_2=1.7$ meV, respectively (now defined by the c axis and the $\langle 11-0\rangle$ base diagonal and along the $\langle 11-0\rangle$ direction, see Fig. 1). The lattice distortion changes J_2 considerably because of the change of Mn-O-Mn bond angle in the monoclinic unit cell with its strongly tilted octahedra.

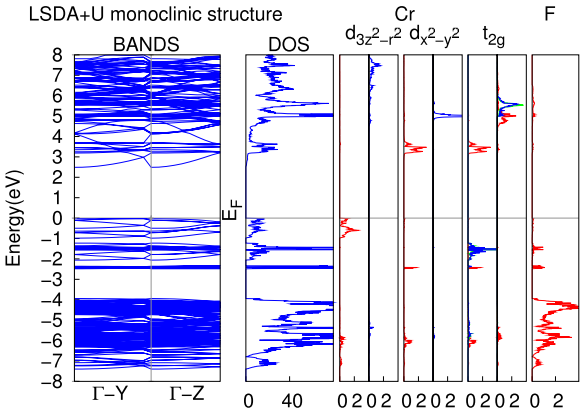

FIG. 10. (Color online) Monoclinic phase of $KCrF_3$: band structure and DOS (per unit cell) calculated in LSDA+U with $U=6.0$ and $J=0.88$ eV. Majority and minority contributions to the DOS for Cr ions and the averaged over all the F ions for p orbitals in the range of [0:4] toward the left and right, respectively, are plotted. Projected density of states corresponding to t_{2g} orbitals d_{xy}, d_{yz}, d_{xz} are shown in the inset (red, green, blue).

Similar to $LaMnO_3$,[30] experimentally, a small spin canting is observed, giving rise to weak ferromagnetism in the monoclinic phase.[8] When the CuF_6 octahedra are tilted, the weak local anisotropy and nonlocal Dzyaloshinskii-Moriya interaction lead to spin canting. In a first principles band structure calculation, this can be taken into account when the relativistic spin-orbit interaction is included on top of the present computation scheme.[11]

V. CONCLUSIONS

With a set of density functional calculations, we have determined the electronic, magnetic and orbital properties of $KCrF_3$. Our ternary chromium fluoride shows many similarities with $LaMnO_3$. From the electronic point of view, the band gap and conduction bandwidth are comparable although somewhat smaller for the more ionic $KCrF_3$ in the orbitally ordered phase. The magnetic structure is of the

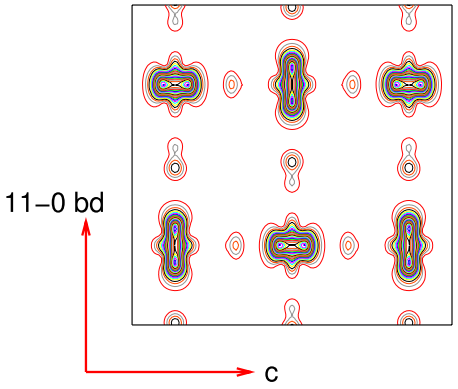

FIG. 11. (Color online) Contour plot of charge density corresponding to the occupied e_g bands below the Fermi level for the monoclinic structure of $KCrF_3$ in LSDA+U.

same A type and the exchange constants are of the same order of magnitude. The orbital ordering in the ferromagnetic planes is identical in the two compounds, although the stacking of the ordering along the *c* axis is different. These properties of $KCrF_3$ make it a material that is comparable to $LaMnO_3$, and it is attractive to investigate, for instance, its orbital excitations[28,31–33] and orbital scattering in photoemission.[34] Doping the strongly correlated Mott insulator $KCrF_3$ with electrons or holes may lead to very interesting prospects, as the equivalent manganites show an overwhelming wealth in physical properties. If the concentration and kinetic energy of the doped carriers suffice a melting of orbital ordering is anticipated, establishing an orbital liquid phase, changing the electronic dimensionality from effectively 2 to 3.[6,35] In the manganites, a colossal magnetoresistance is observed in the vicinity of such a phase transition.

ACKNOWLEDGMENTS

This work was financially supported by "NanoNed," a nanotechnology program of the Dutch Ministry of Economic Affairs, and by the "Nederlandse Organisatie voor Wetenschappelijk Onderzoek (NWO)" and the "Stichting voor Fundamenteel Onderzoek der Materie (FOM)." Part of the calculations was performed with a grant of computer time from the "Stichting Nationale Computerfaciliteiten (NCF)." This paper was supported in part by the National Science Foundation under Grant No. PHY05-51164.

[1] S. Jin, T. H. Tiefel, M. McCormack, R. A. Fastnacht, R. Ramesh, and L. H. Chen, Science **264**, 413 (1994).
[2] M. Imada, A. Fujimori, and Y. Tokura, Rev. Mod. Phys. **70**, 1039 (1998); Y. Tokura and N. Nagaosa, Science **288**, 462 (2000).
[3] A. J. Millis, P. B. Littlewood, and B. I. Shraiman, Phys. Rev. Lett. **74**, 5144 (1995).
[4] Jooss *et al.*, Proc. Natl. Acad. Sci. U.S.A. **104**, 13597 (2007).
[5] C. Zener, Phys. Rev. **82**, 403 (1951); P. W. Anderson and H. Hasegawa, *ibid.* **100**, 675 (1955); P. G. deGennes, *ibid.* **118**, 141 (1960).
[6] For a review, see J. van den Brink, G. Khaliullin, and D. Khomskii, in *Colossal Magnetoresistive Manganites*, edited by T. Chatterji (Kluwer Academic, Dordrecht, 2004).
[7] J. van den Brink and D. Khomskii, Phys. Rev. Lett. **82**, 1016 (1999); J. van den Brink, G. Khaliullin, and D. Khomskii, *ibid.* **83**, 5118 (1999); **86**, 5843 (2001); J. van den Brink and D. Khomskii, Phys. Rev. B **63**, 140416(R) (2001).
[8] S. Margadonna and G. Karotsis, J. Am. Chem. Soc. **128**, 16436 (2006).
[9] S. Margadonna and G. Karotsis, J. Mater. Chem. **17**, 2013 (2007).
[10] J. B. Goodenough, *Magnetism and Chemical Bond* (Interscience, New York, 1963).
[11] I. Solovyev, N. Hamada, and K. Terakura, Phys. Rev. Lett. **76**, 4825 (1996).
[12] S. Satpathy, Z. S. Popovic, and F. R. Vukajlovic, Phys. Rev. Lett. **76**, 960 (1996).
[13] R. Tyer, W. M. Temmerman, Z. Szotek, G. Banach, A. Svane, L. Petit, and G. A. Gehring, Europhys. Lett. **65**, 519 (2003).
[14] Y. Murakami, H. Kawada, H. Kawata, M. Tanaka, T. Arima, Y. Moritomo, and Y. Tokura, Phys. Rev. Lett. **80**, 1932 (1998); Y. Murakami *et al.*, *ibid.* **81**, 582 (1998).
[15] P. Benedetti, J. van den Brink, E. Pavarini, A. Vigliante, and P. Wochner, Phys. Rev. B **63**, 060408(R) (2001).
[16] A. I. Liechtenstein, V. I. Anisimov, and J. Zaanen, Phys. Rev. B **52**, R5467 (1995).
[17] R. Caciuffo, L. Paolasini, A. Sollier, P. Ghigna, E. Pavarini, J. van den Brink, and M. Altarelli, Phys. Rev. B **65**, 174425 (2002).
[18] Z. Nussinov, M. Biskup, L. Chayes, and J. van den Brink, Europhys. Lett. **67**, 990 (2004).
[19] P. Hohenberg and W. Kohn, Phys. Rev. **136**, B864 (1964); W. Kohn and L. J. Sham, Phys. Rev. **140**, A1133 (1965).
[20] D. M. Ceperley and B. J. Alder, Phys. Rev. Lett. **45**, 566 (1980).
[21] G. Kresse and J. Furthmuller, Phys. Rev. B **54**, 11169 (1996); Comput. Mater. Sci. **6**, 15 (1996).
[22] D. Khomskii and J. van den Brink, Phys. Rev. Lett. **85**, 3329 (2000).
[23] Cococcioni and S. de Gironcoli, Phys. Rev. B **71**, 035105 (2005).
[24] W. E. Pickett, S. C. Erwin, and E. C. Ethridge, Phys. Rev. B **58**, 1201 (1998).
[25] M. S. Hybertsen, M. Schluter, and N. E. Christensen, Phys. Rev. B **39**, 9028 (1989).
[26] K. I. Kugel and D. I. Khomskii, Sov. Phys. Usp. **25**, 231 (1982).
[27] G. Khaliullin and V. Oudovenko, Phys. Rev. B **56**, R14243 (1997).
[28] J. van den Brink, P. Horsch, F. Mack, and A. M. Oles, Phys. Rev. B **59**, 6795 (1999).
[29] J. van den Brink, New J. Phys. **6**, 201 (2004).
[30] V. Skumryev, F. Ott, J. M. D. Coey, A. Anane, J.-P. Renard, L. Pinsard-Gaudart, and A. Revcolevschi, Eur. Phys. J. B **11**, 401 (1999).
[31] E. Saitoh, S. Okamoto, K. T. Takahashi, K. Tobe, K. Yamamoto, T. Kimura, S. Ishihara, S. Maekawa, and Y. Tokura, Nature (London) **410**, 180 (2001).
[32] V. Perebeinos and P. B. Allen, Phys. Rev. Lett. **85**, 5178 (2000).
[33] J. van den Brink, Phys. Rev. Lett. **87**, 217202 (2001).
[34] J. van den Brink, P. Horsch, and A. M. Oles, Phys. Rev. Lett. **85**, 5174 (2000).
[35] J. van den Brink, Nat. Mater. **5**, 427 (2006).